Archives of Mechanics • Archiwum Mechaniki Stosowanej • 28, 5–6, pp. 733–758, Warszawa 1976

Numerical study of nonequilibrium processes in two-dimensional turbulent reactive gas flows

V. I. GOLOVICHEV, N. G. PREOBRAZHENSKY AND V. A. YASAKOV
(NOVOSIBIRSK)

The results of nonequilibrium process analyses for turbulent reactive shear flows designed for rapid mixing are presented in the paper. The chemical systems consisted of hydrogen and air as well as hydrogen and fluorine have been studied numerically in the turbulent mixing zone formed between two coaxial streams. The basic conservation equations for a chemically reacting multi-component gas flows, their thermophysical, turbulent transport and optical properties are discussed in details. The analysis is performed by applying a modified version of the Cranck-Nicolson type implicit finite-difference scheme that incorporates the net with non-uniform spacing grids to minimize the truncation errors, and quasi-linearization techniques. The principal intention of this study is to reveal the macroscopic behaviour of the finite-rate oxidation process in the hydrogen-air system, and to analyze parametrically the optimum operating conditions for the chemically pumped turbulent flow CW HF-laser.

W pracy przeprowadzono analizę procesów nierównowagi w turbulentnych przepływach chemicznie aktywnego ścinanego gazu, celem zbadania warunków szybkiego burzliwego mieszania gazów. Związki chemiczne składające się z wodoru i powietrza bądź wodoru i fluoru badano numerycznie w turbulentnej strefie mieszania utworzonej z dwóch współosiowych strumieni. Szczegółowo przedyskutowano podstawowe równania zachowania dla przepływów chemicznie aktywnych gazów wieloskładnikowych, ich równania termofizyczne transportu w strefie burzliwej oraz własności optyczne. Do obliczeń przyjęto zmodyfikowaną wersję schematu różnicowego typu Crancka-Nicolsona zawierającego siatkę z nierównomiernym podziałem oczek celem zmniejszenia do minimum błędów obcięcia i quasi-linearyzacji równań. Głównym celem pracy było wykrycie prawidłowości w procesie utleniania ze skończoną prędkością zachodzącego w związku wodorowo-powietrznym i określenie parametrów, przy których występują optymalne warunki dla turbulentnego przepływu w laserach chemicznych CW i HL.

В работе проведен анализ неравновесных процессов в сдвиговых турбулентных течениях химически активного газа с целью исследования условий быстрого смешивания газов. Химические соединения, состоящие из водорода и воздуха или водорода и фтора, исследованы численно в турбулентной зоне смешивания, образованной двумя соосными потоками. Подробно обсуждены основные уравнения сохранения для течений химически активных многокомпонентных газов, их термофизические свойства, перенос в зоне смешения и оптические свойства. Для расчетов принят модифицированный вариант разностной схемы типа Кранка-Никольсона, содержавший сетку с неравномерным распределением ячеек с целью уменьшения к минимуму ошибок усечения и квазилинеаризацию уравений. Главной целью работы являлось вскрытие закономерностей в процессе окисления с конечной скоростью, происходящего в водоро-воздушной смеси и определение параметров, при которых возникают оптимальные условия для работы турбулентного HF-химического лазера непрерывного действия.

1. Introduction

A QUANTITATIVE analysis of nonequilibrium processes in turbulent chemically active gas flows appears to be of a great importance in relaxation gasdynamics. Basing on such an analysis it seems to be possible to elucidate a role of finite rate processes associated

with some specific nonequilibrium phenomena. Certain finite rate processes are likely to be very important themselves as well as due to their coupling and interplays. For example, the jet propulsion developments and high-speed convective flows CW laser problems are associated with extensive studies of flow systems with initially separated reactants, e.g., of Diffusion Chemical Reactors (DCR). For these systems of interest an analysis is required of various nonequilibrium phenomena contributions in: 1) fuel and oxidizer mixing; 2) generation of turbulence due to evolutions of the averaged flowfield parameters during the supersonic nozzle expansion, 3) chemical transformations and 4) molecular energy transfer between different modes of the reaction produced excited molecules.

For the combustion process descriptions, theoretical models are necessary to be developed which could account the temperature and mixing dynamics in the finite rate reacting flows to describe the ignition or quenching phenomena. For the CW diffusion chemical laser operation, the mixing rate should be sufficiently faster than the both collisional deactivation and convective flow rates to provide an effective transformation of chemical energy into the stimulated light emission, while the characteristic time of the cavity flow exchange of a lasing gas should be of the same order of value as lifetimes of inverted levels of active molecules or "donors" in the premixed systems.

The primary problem in theoretical modeling of such systems is the formulation of additional constitutive equations for basic variables participating in the relaxation process as well as obtaining the proper "dissipative" coefficients to be included in the fundamental system of conservation equations. The corresponding relations are written in a form of parabolic partial derivatives under conditions that the standard mathematical treatment is to be valid. An accurate solution of such a problem has only a principal discrepancy associated with the non-adequate representation of a real physical process by their formal treatment. Such an "exact" solution seems to be a more instructive one rather than the approximated approach thus giving a possibility of judging the theoretical model validity and obtaining quantitative details of relaxation processes.

The development of the solution procedure for governing mathematical system constitutes an important part of this investigation, and it will be discussed separately.

The chemical systems chosen in this study are hydrogen and air or hydrogen and fluorine. The structure of a turbulent mixing zone between two coaxial streams of initially separated reactants is analyzed numerically and the results illustrate some typical examples of macroscopic behavior of a hydrogen jet inflammation in air as well as the parametrical analyses of the optimum operating conditions for a supersonic turbulent mixed flow HF-chemical laser.

2. Formulation

2.1.

A two-dimensional cylinder coordinate system (x, y, or r) is analyzed. The single nozzle/injector flow configuration designed for fast mixing is shown in Fig. 1. Such a flow geometry provides inherently faster mixing characteristics as compared to the proper slot system. Two parallel non-uniform and confined gas streams, containing oxidant or fuel plus diluent or reaction intermediates are subjected to a supersonic motion under

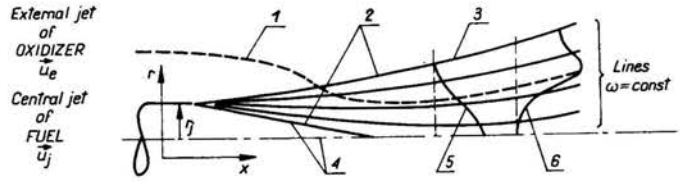

FIG. 1. Flow model and coordinate system.

1) sample of streamline, 2) boundaries of a mixing zone, 3) E-boundary, 4) I-boundary, 5, 6) profiles of flow paramters.

condition of the well developed turbulent flow regime. One of the gas streams is usually activated by means of a temperature rise together with an increase in active intermediate concentrations.

Basic equations of the phenomenological turbulent boundary layer theory of the chemically reacting, heat-conducting N-species gas mixture are employed to describe simultaneously the convective and turbulent transfer of mass, momentum and energy. It is assumed that the gas flow is shock-free, and the mixture is the perfect and ideal gas medium.

The turbulence concept in phenomenological fluid dynamics theories is adequate for a correlation presence between flow parameters on divers hydrodynamic scales. While postulating these correlations in a specific form that reduces to the turbulent viscosity model, the spatial fluxes of mass, momentum and energy associated with the turbulent exchange can be determined as being dependent on time averaged values of unknown variables in governing equations as follows:

$$-\langle(\varrho v)' Y_i'\rangle = \mu_t Sc_{t,i}^{-1}(\partial\langle Y_i\rangle/\partial y),$$

$$-\langle(\varrho v)' u'\rangle = \mu_t(\partial\langle u\rangle/\partial y),$$

$$-\langle(\varrho v)' \sum_{i=1}^{N}\langle Y_i'\rangle h_i'\rangle = \mu_t Pr_t^{-1}(\partial\langle h\rangle/\partial y).$$

The sign $\langle\ \rangle$ denotes a time-averaged quantity; u, v are the mean velocity components in the x and y directions; h, h_i are static enthalpies per unit mass for the whole mixture and the i-species, respectively; μ_t is the effective turbulent viscosity coefficient.

After assuming the Pr_t, $Sc_{t,i}$ number values to be constant ($Pr_t = 0.85$, $Sc_{t,i} = Pr_t^{-1}$), the specification of the turbulent transport properties is reduced to the effective turbulent viscosity coefficient description that is a function of the averaged flowfield parameters. Hence the analyzed system is formally similar to the conservation laws as presented in [1], with the effective turbulent transport coefficients replacing their molecular equivalents. If the classical Prandtl turbulent viscosity model expressed in terms of a "mixing length" is employed,

$$\mu_t = \chi_1 \varrho l_t(\partial\langle u\rangle/\partial y) \tag{2.1}$$

it includes an assumption of some level of turbulence to be established instantly in accordance with the development of an averaged profile of the flowfield parameters. Thus, the history of the flow development is ignored while it is necessary to consider the initial turbulence level as well as the turbulence produced in the course of jet interactions. It should also be kept in mind that the use of the above written expression with regard to jets hav-

ing equal velocities leads to unreal, i.e., very low mixing rates. Consequently, the model of the effective turbulent viscosity has been as proposed in [2] basing on the treatment of experimental data obtained for nonreacting coaxial jets of dissimilar gases

$$\mu_t = \chi_1 \varrho u_j (1-\lambda)^2 (x+\chi_2). \tag{2.2}$$

Here χ_1, χ_2 are the "universal" constants for a given flow geometry, $\lambda = u_e/u_j$ is the ratio of the mixing streams velocities.

Together with the model (2.2) a simple "two-equation" model, $k \sim \varepsilon$, with some modifications for axisymmetrical flows was employed. In this model, the effective turbulent viscosity is related to k-turbulent kinetic energy, and ε is its dissipation rate via dimensional expression

$$\mu_t = c\mu \varrho k^2/\varepsilon, \tag{2.3}$$

where ϱ is the density of fluid.

This model is proved to present the best predictions for the jet flow geometry. In order to complete the fundamental turbulent boundary layer system, two additional equations were added similarly to [3]. These equations allow for the quantities k and ε to be changed through convective and diffusive transport and energy exchange between the mean and fluctuating flows. Other models are classified by means of a number of supplmentary equations used to complete the problem. One can find in [4] the extensive review on such a topic to be useful. Formally, the effect of nonequilibrium chemical reactions that creates the vibrationally excited product molecules is generally accounted for by introducing the source terms, or the relaxation function, in the macroscopic mass balance equations. Each of the long-lived vibrational levels of the active molecule should be treated in this case as a separate component of a gas mixture. The source term is formed according to the stoichiometric relation

$$\sum_{i=1}^{N} \nu'_{ij} X_i \underset{K_b^j}{\overset{K_f^j}{\rightleftarrows}} \sum_{i=1}^{N} \nu''_{ij} X_i, \quad j = 1, \ldots, S,$$

which is based on the mass equilibrium law as it is employed in chemical kinetics:

$$\begin{aligned} \langle \dot{w}_i \rangle &= \sum_{j=1}^{S} \langle \dot{w}_{ji} \rangle; \quad \langle \dot{w}_{ji} \rangle = W_i (\nu''_{ij} - \nu'_{ij}) \langle \dot{R}_j \rangle, \\ \langle \dot{R}_j \rangle &= K_f^j(\langle T \rangle) \prod_{i=1}^{N} \langle c \rangle^{\nu'_{ij}} - K_b^j(\langle T \rangle) \prod_{i=1}^{N} \langle c \rangle^{\nu''_{ij}}, \\ \langle c_i \rangle &= \langle \varrho Y_i \rangle / W_i. \end{aligned} \tag{2.4}$$

Here W_i is the molecular weight of the i-th species; ν'_{ij}, ν''_{ij} are the stoichiometric coefficients of the i-th species in the j-th reaction for reactants and products, respectively; and Y_i is the mass concentration of the i-th species. It is assumed that the source term written in the specific form (2.4) is not changed in the turbulent flow.

2.2.

The solution of the conservation equations in a reacting boundary layer can be sufficiently simplified if the dependent and independent variables transformations are used.

This mathematical problem is well-known, and possible difficulties are associated with the fact that the character of a boundary-value problem is not regular. The conservation equations contain the independent variable, x, by means of which the problem becomes the Cauchy one, but the derivative, $\partial(\varrho v)/\partial x$, is not present in the basic equations. In order to exclude the ϱv-function, the von Mises transformation is used; it defines the relation of the stream function $\psi = \int_0^y (\varrho u) r^\alpha dy$, to momentum components in a form:

$$\varrho u r^\alpha = \frac{\partial \psi}{\partial y}, \qquad -(\varrho v + \langle \varrho' v' \rangle) r^\alpha = \frac{\partial \psi}{\partial x}, \qquad \alpha = 0, 1.$$

Hence, the total mass conservation equation is satisfied identically, and the "normal" boundary-value problem formulation is valid. An introduction of the nondimensional stream function, ω, as the cross-stream variable similarly to [5], but with $\gamma \neq 1$

$$\omega = \left[\int_0^y \varrho u r^\alpha dy / (\psi_E - \psi_I)^{1/\gamma} \right]$$

transforms, in general, the boundary layer region to the rectangular one of the unit height. The algorithm of the numerical integration in this case is proved to be the most simple and efficient procedure. The subscripts I and E, denote the inner and outer boundaries of the calculated region where the unknown dependent variables are changed to a sufficient degree. In the von Mises coordinate system (x, ω), the basic conservation equations are represented in a generalized form

$$\partial \phi / \partial x + (a + b\omega^\gamma) \partial \phi / \partial \omega = \partial (c \partial \phi / \partial \omega) / \partial \omega + \Omega_\phi. \tag{2.5}$$

The coefficients a, b, c have the following meanings:

$$a = \frac{r_I^\alpha \dot{m}_I}{\gamma \omega^{\gamma-1} (\psi_E - \psi_I)}, \qquad b = \frac{r_E^\alpha \dot{m}_E - r_I^\alpha \dot{m}_I}{\gamma \omega^{\gamma-1} (\psi_E - \psi_I)}, \qquad c = \frac{r^{2\alpha} \varrho u \mu_t \sigma_{t,\phi}^{-1}}{(\gamma \omega^{\gamma-1} (\psi_E - \psi_I))^2}.$$

Here $\sigma_{t,\phi}$ is the transport coefficient that characterizes the turbulent exchange (Pr_t or $Sc_{t,i}$). The quantities $r_I^\alpha \dot{m}_I$ and $r_E^\alpha \dot{m}_E$ denote the gradients of mass fluxes through I and E boundaries, respectively, of the calculating region with obvious definitions:

$$r_G^\alpha m_G = \lim_{\substack{\omega \to \omega_I \\ \omega \to \omega_E}} \gamma \omega^{\gamma-1} (\psi_E - \psi_I) \frac{\partial (c \partial \phi / \partial \omega) / \partial \omega}{\partial \phi / \partial \omega}. \tag{2.6}$$

The finite-difference version of (2.6) is seen to be finite when determined from the expression of effective turbulent viscosity in the form (2.2) and (2.3), and it is used to calculate a rate of the mixing layer development. The quantity Ω_ϕ stands for the "source term" associated with the corresponding equation. Table 1 clarifies the particular meaning of ϕ with respect to different variables in basic equations.

Special attention should be paid to the effective approximation of the nonlinear terms (2.4) in Ω_ϕ that take into account the mass production in the course of a chemical reaction. It is well-known, [6–7] that the fast chemical reactions make it necessary to introduce small dimensionless parameters, ratios of the specific chemical reaction times in the high temperature region to the characteristic hydrodynamic time scale. A similar situation is always encountered in the problems of nonequilibrium gasdynamics when the short-

Table 1. The system of governing Eq. (2.5)

CONSERVATION LAW	VARIABLE ϕ	TRANSPORT PROPERTY Γ_ϕ	SOURCE TERM Ω_ϕ
MOMENTUM IN x-DIRECTION	VELOCITY u	TURBULENT VISCOSITY μ_t	PRESSURE GRADIENT $-\frac{dP}{dx}\Big/\rho u$
CHEMICAL SPECIES i	MASS CONCENTRATION Y_i	TURBULENT DIFFUSIVITY $\mu_t/Sc_{t,i}$	CHEMICAL REACTION RATE $\dot{w}_i/\rho u$
AVERAGE TURBULENT FLOW ENERGY	STAGNATION ENTHALPY $H=\sum_{i=1}^{N} h_i(T)Y_i + (u^2/2)+K$	TURBULENT DIFFUSIVITY μ_t/Pr_t	$\frac{\partial}{\partial\omega}\left\{C\left[(1-Pr_t)\frac{\partial}{\partial\omega}\left(\frac{u^2}{2}\right)+ + C\,Pr_t Pr_{t,K}^{-1}(1-Pr_{t,K})\frac{\partial K}{\partial\omega}\right]\right\}$
TURBULENCE KINETIC ENERGY	$K=\langle u'u'\rangle^2/2$	TURBULENT DIFFUSIVITY $\mu_t/Pr_{t,K}$	$Pr_{t,K}C\left(\frac{\partial u}{\partial\omega}\right)^2 - C_\mu\frac{\rho K^2}{\mu_t u}$
TURBULENCE KINETIC ENERGY DISSIPATION RATE	$\varepsilon=\nu\left\langle\frac{\partial u'}{\partial y}\frac{\partial u'}{\partial y}\right\rangle$	TURBULENT DIFFUSIVITY $\mu_t/Pr_{t,\varepsilon}$	$Pr_{t,\varepsilon}CC_1C_\mu K\left(\frac{\partial u}{\partial\omega}\right)-C_2\frac{\varepsilon^2}{Ku}$

NOTE: $C=r^{2\alpha}\rho u\mu_t\sigma_{t,\phi}^{-1}\Big/\gamma\omega^{\gamma-1}(\psi_\varepsilon-\psi_I)^2$;

COEFFICIENCES IN MODELS OF TURBULENCE ARE:

1. MODEL, [2] — $\chi_1=2.75\cdot10^{-5}$, $\chi_2=0.075$;
2. MODEL, [3] — $C_\mu=0.09-0.04f$, $C_1=1.44$, $C_2=1.92-0.0667f$,
$Pr_{t,K}=1.0$, $Pr_{t,\varepsilon}=1.3$, $f=\left|\frac{1}{2}\frac{r_\varepsilon-r_I}{u_\varepsilon-u_I}\left(\frac{\partial u_\varepsilon}{\partial x}-\left|\frac{\partial u_\varepsilon}{\partial x}\right|\right)\right|$.

living active particles (e.g., atoms, radicals) participate in the reaction as being introduced in a kinetic scheme to explain the reaction mechanism. In a steady-state numerical problem, the different rates of the chemical mass production are manifested in the differences in scales of the subsequent derivatives, $\partial\Omega_\phi/\partial\phi$. This difference of scale presents of some difficulty for the computation procedure since it is considered to be necessary to approximate either weakly or strongly damping terms in order to get a satisfactory approximation of solution when employing the explicit methods. Practically, this means that the step size of the difference grid is determined by the fastest stage of the chemical process, while the integration interval is determined by the slowest one, it results in an excessive computing time. At present, there is no generally accepted method for solving the combined systems of gasdynamic and kinetic equations. This fact seems to be in line with narrow trends in such topics as well as the result of the algorithms complexity. A wide class of algorithms is based on the use of implicit difference schemes together with the quasi-linearization (linearization) techniques that provide useful computation procedures and fast (quadratic) convergences [8].

A similar approximation of the initial problem leads to a sequence of linear equations re-arranged in the form

$$\phi^{l,m} = A_\phi^{l-1,m+1}\phi^{l,m+1} + B_\phi^{l-1,m-1}\phi^{l,m-1} + C_\phi^{l-1,m} \tag{2.7}$$

and solved by a simple recurrence formula. Here l, m are the mesh indexes of the finite-difference grid, $(x_t, \omega_m)_\Delta$.

The finite-difference form of the source term Ω_ϕ in Eq. (2.5) is presented as follows:

$$\Omega_\phi^{l,m} = \tilde{\Omega}_\phi^{l-1,m} + \dot{\Omega}_\phi^{l-1,m} \cdot \phi^{l,m}, \tag{2.8}$$

where the "generation" terms ϕ do not contain ϕ are grouped in $\tilde{\Omega}_\phi^{l-1,m}$. It is obvious that $\tilde{\Omega}_\phi \geqslant 0$ and $\dot{\Omega}_\phi \leqslant 0$. From the linear recurrent-formulae for mass balance equations, the condition of a non-negative solution is easily obtained by means of the linear interpolation, the latter determines the form of the source term approximation, namely as $\tilde{\Omega}_\phi \geqslant 0$. The algorithm as described above has the following useful computation properties:

The algorithm gives the stable approximate solutions not oscillating for the rapidly changed variables independent of the step size integration employed.

The algorithm preserves a "band" matrix structure for approximation systems of the linear algebraic equations which is determined by the relation for the finite-difference approximation of derivatives in the initial differential equations.

The algorithm allows for integrating with the automatic step size control, the transversal size of the finite-difference grid (when preserving the mesh quantity), and the longitudinal step size of integration being changed with regard to the rate of growth of a mixing layer in such a way that it leads to a smooth distribution of the calculated parameter.

2.3.

The chemical equilibrium conditions were assumed in plenum chamber calculations of the mixture composition and thermal conditions in the activated reactant stream. Combustion preheating of the centrally positioned hydrogen jet is employed to insure the autoignition of the mixture in the mixing layer which is formed between two coaxial jets. As a result of preheating, the active intermediates and water vapour are present in the central jet. The effect of these admixtures on the ignition process development is proved to be rather essential [9]. In a supersonic diffusion laser (SDL) which exploits the nonbranched chain reaction between atomic fluorine and molecular hydrogen in the mixing and reacting layer, an activated mixture, $F_2/H_2/He(N_2)$ provides the thermal conditions for the laser operation in a "cold" pumping regime. An expansion of the preburned products through a supersonic 15-degree half-angle cone nozzle is used to "freeze" the reaction so as to obtain high levels of atomic fluorine concentrations to be available in the downstream reacting cavity flow. These calculated expansion parameters are taken to be initial ones in the mixing zone for calculating the reacting boundary layer equations.

3. Results and discussion

3.1. Ignition of a hydrogen jet in air

The conservation equation, (2.5), is integrated numerically by means of the method described above for one geometrical flow configuration when varying the parameters of the mixing reagents streams: their compositions (activation degrees), velocities, temper-

atures and pressures. As a studied gas medium a mixture of an inert non-dissociated nitrogen and oxygen which dissociates and reacts with hydrogen according to the scheme given in Table 2 is used. The mixture consists of eight reacting components, H, O, H_2O, OH, O_2, H_2, HO_2, H_2O_2, which take part in 20 elementary stages. The first nine stages were suggested in the Duff's model [10] and were widely used in similar calculations. Two sets (I, II) of the reaction rates coefficients were considered as presented in Table 2. The coefficients used in set I are mainly the same as in [11]. The coefficients of set II and the next stages were taken according to recommendation of [12]. Figure 2 illustrates the effect of the usage of the modernized kinetic data for bimolecular change reactions to be manifested in the ignition lag decrease of the homogeneous mixture in the low temperature region, while an opposite influence is observed at high temperatures. Figure 3a illustrates the results of the HO_2 and H_2O_2 influence, these species being included in the scheme chain to explain the reaction mechanism of hydrogen oxidation at high pressures and low temperatures, thus exerting the ignition character of hydrogen jet preheated by combustion in air (Case 1, Table 3). This figure shows axial distributions of the complete mixture composition and gas temperatures with and without inclusion of HO_2 and H_2O_2 into the reaction model.

Figure 3b presents the radial profiles of the same parameters across the flowfield in one axial position. When comparing the concentration levels of HO_2 and H_2O_2 for the two cases one can conclude that the availability of these components in the reacting mixture is seen to be essential in the relatively narrow side jet region at a temperature less than 1000 °K. The peak values of axial concentrations of HO_2 and H_2O_2 in this region can exceed all the other active radicals' concentrations. The reactions of thermal decomposition of these species (reverse stages of reactions 10 and 20) play an essential part at high temperatures. The radial temperature profiles have typical maxima in the diffusion combustion. A noticeable temperature decrease appears due to quenching by a cold oxidation atmosphere at a starting part of the mixing zone. This zone can be observed in the direct flame photographs of the diffusion flame as shown in Fig. 4. At constant λ the

Table 1. Chemical model for the hydrogen — air system.

REACTION No.	REACTION	REACTION RATE COEFFICIENTS *) FORWARD	BACKWARD
1	$H + O_2 \rightleftharpoons OH + O$	$3.0 \times 10^{14} e^{-8.81/T}$ ($2.24 \times 10^{14} e^{-8.844/T}$)	$2.48 \times 10^{13} e^{-0.66/T}$ (1.3×10^{13})
2	$O + H_2 \rightleftharpoons OH + H$	$3.0 \times 10^{14} e^{-4.03/T}$ ($1.74 \times 10^{13} e^{-4.76/T}$)	$1.3 \times 10^{14} e^{-2.49/T}$ ($7.33 \times 10^{13} e^{-3.67/T}$)
3	$H_2 + OH \rightleftharpoons H + H_2O$	$3.0 \times 10^{14} e^{-3.02/T}$ ($2.19 \times 10^{13} e^{-2.59/T}$)	$1.33 \times 10^{15} e^{-10.95/T}$ ($8.41 \times 10^{13} e^{-10.57/T}$)
4	$2\,OH \rightleftharpoons O + H_2O$	$3.0 \times 10^{14} e^{-3.02/T}$ ($5.75 \times 10^{12} e^{-0.394/T}$)	$3.12 \times 10^{15} e^{-12.51/T}$ ($5.75 \times 10^{13} e^{-9.47/T}$)
5	$H_2 + M \rightleftharpoons 2H + M$	$1.35 \times 10^{17} e^{-54/T}$ ($2.4 \times 10^{19} e^{-61.518/T}/T^2$)	1.0×10^{16} ($7.5 \times 10^{15}/T$)
6	$H_2O + M \rightleftharpoons OH + H + M$	$9.66 \times 10^{18} e^{-62.2/T}/T$ (3.4×10^{5})	1.0×10^{17} ($9.26 \times 10^{16}/T$)
7	$OH + M \rightleftharpoons O + H + M$	$8.0 \times 10^{16} e^{-52.2/T}/T$ ($2.02 \times 10^{18} e^{-52.0/T}/T^2$)	1.0×10^{16} ($2.0 \times 10^{15}/T$)
8	$O_2 + M \rightleftharpoons 2O + M$	$5.8 \times 10^{16} e^{-60.6/T}/T$ ($5.8 \times 10^{16} e^{-60.6/T}/T$)	6.0×10^{14} (6.0×10^{14})
9	$H_2 + O_2 \rightleftharpoons 2\,OH$	$2.72 \times 10^{13} e^{-29.2/T}$ ($1.0 \times 10^{16} e^{-35.2/T}$)	$8.34 \times 10^{10} e^{-10.32/T}$ ($3.42 \times 10^{14} e^{-26.61/T}$)

*) SET II RATE COEFFICIENTS ARE IN PARENTHESES.

Table 2. (cont.) Possible reactions involving HO_2 and H_2O_2

REACTION No.	REACTION	REACTION RATE COEFFICIENTS *)	
		FORWARD	BACKWARD
10	$HO_2 + M \rightleftharpoons H + O_2 + M$	$2.4 \times 10^{15} e^{-23.1/T}$	$1.59 \times 10^{15} e^{0.203/T}$
11	$HO_2 + H_2 \rightleftharpoons H_2O_2 + H$	$9.6 \times 10^{12} e^{-12.1/T}$	$2.34 \times 10^{13} e^{-4.63/T}$
12	$HO_2 + H_2 \rightleftharpoons OH + H_2O$	$1.0 \times 10^{11} e^{-12.0/T}$	$1.65 \times 10^{9} e^{-27.6/T}$
13	$HO_2 + H \rightleftharpoons OH + OH$	$2.5 \times 10^{14} e^{-0.95/T}$	$1.2 \times 10^{13} e^{-20.2/T}$
14	$HO_2 + O \rightleftharpoons OH + O_2$	1.0×10^{13}	$7.5 \times 10^{12} e^{-28.0/T}$
15	$HO_2 + OH \rightleftharpoons H_2O_2 + O$	$2.0 \times 10^{12} e^{-10.6/T}$	$2.8 \times 10^{13} e^{-3.2/T}$
16	$HO_2 + OH \rightleftharpoons H_2O + O_2$	3.0×10^{14}	$2.3 \times 10^{12} e^{-36.6/T}$
17	$HO_2 + H_2O \rightleftharpoons OH + H_2O_2$	$2.8 \times 10^{13} e^{-16.45/T}$	$1.0 \times 10^{13} e^{-0.906/T}$
18	$H_2O + OH \rightleftharpoons H_2O_2 + H$	$8.5 \times 10^{12} e^{-0.5/T}$	$2.2 \times 10^{12} e^{-21.07/T}$
19	$HO_2 + HO_2 \rightleftharpoons H_2O_2 + O_2$	$5.6 \times 10^{13} e^{-39.0/T}$	$3.18 \times 10^{14} e^{-4.53/T}$
20	$H_2O_2 + M \rightleftharpoons OH + OH + M$	$1.17 \times 10^{17} e^{-22.9/T}$	$8.4 \times 10^{14} e^{+2.67/T}$

*) THE UNITS OF THE RATE COEFFICIENTS ARE: $cm^3 mole^{-1} sec^{-1}$ – FOR BIMOLECULAR REACTIONS, $cm^6 mole^{-2} sec^{-2}$ – TRIMOLECULAR REACTIONS; T IS ABSOLUTE TEMPERATURE IN K DEVIDED BY 1000; M IS A CATALYST.

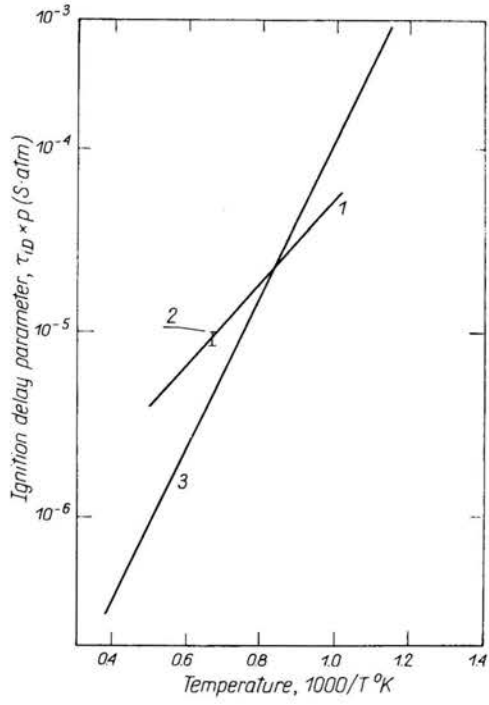

FIG. 2. Correlation of computed ignition delay times for stoichiometric hydrogen-air mixture.

length of the flame separation is increased up to some limit with an increase of the stream velocities (see Fig. 4) after which the hydrogen-air autoignition regime cannot be realized in numerical experiments.

From the formal kinetic point of view, the role of chain-breaking reactions is increased with the mixture pressure that leads to the decomposition of active centers, H, O, OH (reverse stages of reactions, 5–8, 20). Moreover, the role of the reverse stage of the reaction

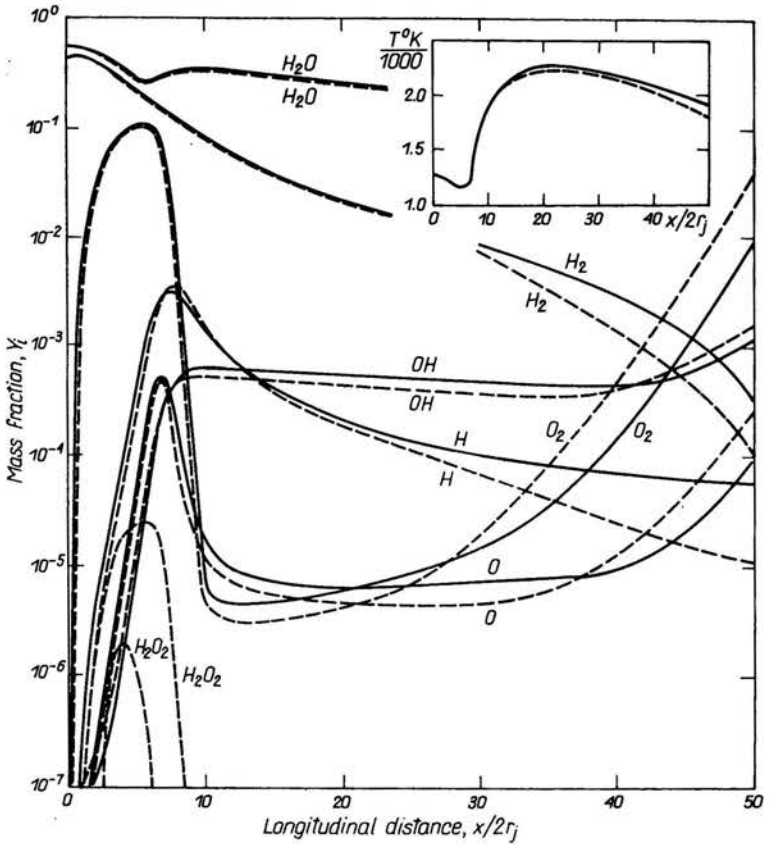

FIG. 3a. Chemical composition and temperature histories along centerline for hydrogen-air mixing with finite rate reactions (Case 1 of Table 3). Dotted lines are for the reacting chain analysis including HO_2 and H_2O_2 species with 20 possible reactions from Table 2. Solid lines refer to the analysis of 9 reactions.

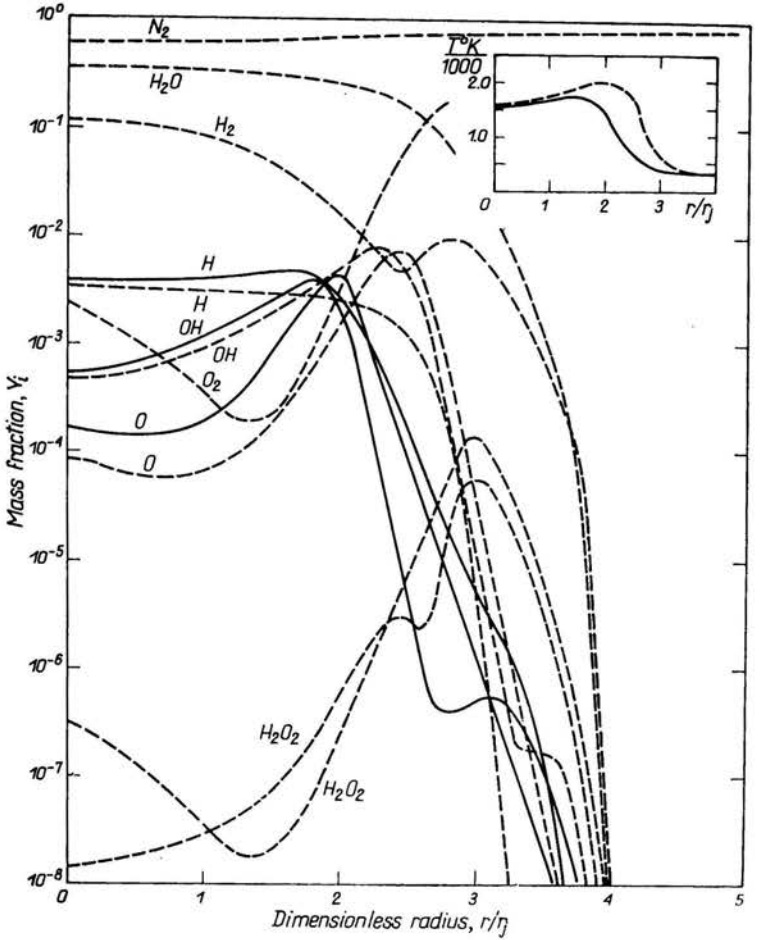

FIG. 3b. Radial chemical composition and temperature profiles at longitudinal distance $x/2r_j = 8$ position for hydrogen-air mixing with finite rate reactions. Initial stream parameters and nomenclature are the same as those for Fig. 3a.

10, due to formation of the less active radical, HO_2, becomes more essential and it increases also the possibility of developing of chains through this radical. Figures 5–6 illustrate the hydrogen hot jet ignition at the elevated pressures (p = 3 atm, Case 2). It is expected that the concentration levels of HO_2 and H_2O_2 turn out to be essentially higher and noticeably exceeding the quantity of active radicals, H, O and OH during the induction stage in the side flow region. The ignition is realized in numerical experiments

Table 3. Initial parameters for mixing streams.

	CASE 1	CASE 2	CASE 3	CASE 4	CASE 5	CASE 6	CASE 7	CASE 8	CASE 9
CENTRAL JET (j)									
MIXTURE COMPOSITION									
MASS FRACTION									
FOR $H_2/O_2/N_2$ FOR $H_2/F/N_2$(He)									
H	1.5×10^{-8}	1.5×10^{-8}	6.72×10^{-6}	–					
O	1.0×10^{-8}	1.0×10^{-8}	5.0×10^{-6}	–					
H_2O	0.5508	0.5508	0.5507	–					
OH	5.0×10^{-9}	5.0×10^{-9}	7.72×10^{-7}	–					
H_2	0.4492	0.4492	0.4492	1.0					
N_2					0.5	0.0	0.0	0.0	0.0
He					0.0	0.0	0.0	0.0	0.0
H_2					0.5	1.0	1.0	1.0	1.0
STATIC TEMPERATURE, °K	1275	1275	1158	1158	300	1000	300	300	300
VELOCITY, m/sec	945	3000	945	945	4004	4004	4004	4004	4004
STATIC PRESSURE, ATM	1.0	3.0	1.0	1.0					
EXTERNAL STREAM (e)									
MIXTURE COMPOSITION									
MASS FRACTION									
O_2	0.232	0.232	0.232	0.232					
N_2	0.768	0.768	0.768	0.768					
N_2					0.5	0.5	0.5	0.0	0.0
He					0.0	0.0	0.0	0.5	0.5
F					0.5	0.5	0.5	0.5	0.35
HF(e)					0.0	0.0	0.0	0.0	0.15
STATIC TEMPERATURE, °K	348	348	348	348	600	1000	600	540	482
VELOCITY, m/sec	160.6	510	160.6	160.6	2288	2288	1500	2288	2288
STATIC PRESSURE, ATM	1.0	3.0	1.0	1.0					

FOR COMBUSTION PROBLEM r_j = 0.635 CM,
FOR HF-CHEMICAL LASER r_j = 0.05 CM.

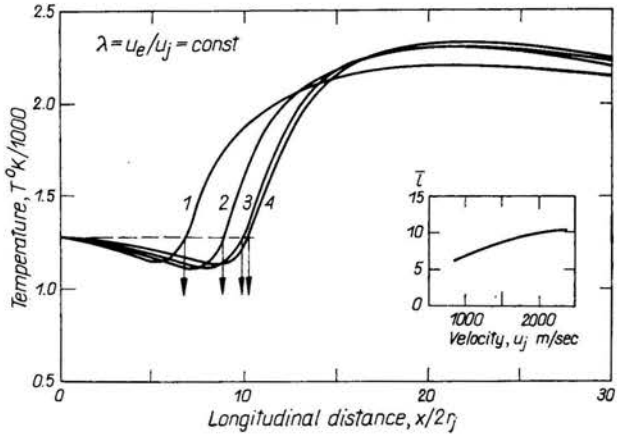

FIG. 4. Centerline temperature profiles and the length of flame separation — jet velocity history for hydrogen-air mixing. The line numeration refers to situations as follows: 1) u_j = 945 m/sec, 2) u_j = = 1500 m/sec, 3) u_j = 2000 m/sec, 4) u_j = 2500 m/sec. The rest parameter sare the same as for Case 1.

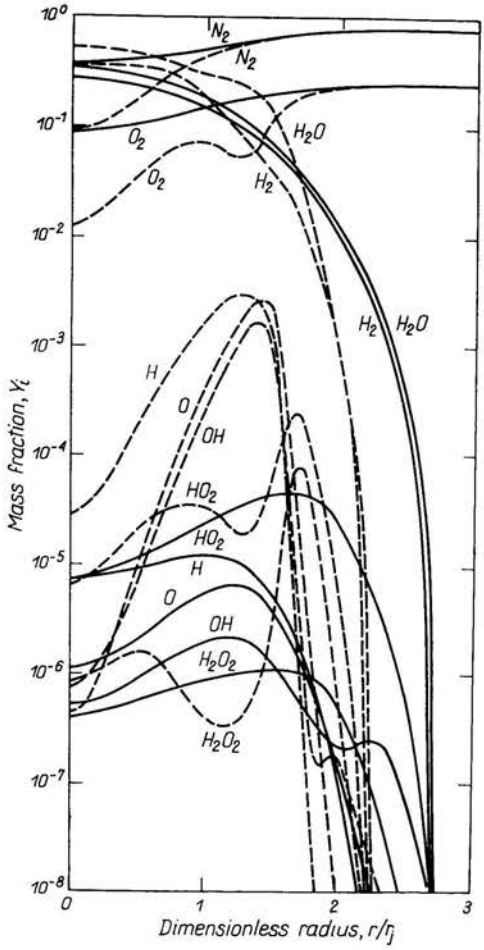

FIG. 5. Radial chemical composition profiles at longitudinal distance $x/2r_j = 4$ position under the condition of different static pressures for hydrogen-air mixing. Solid lines are for Case 1, dotted lines — Case 2.

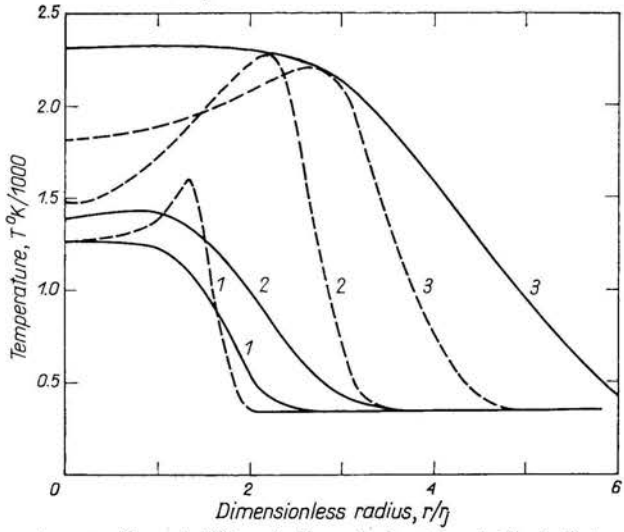

FIG. 6. Radial temperature profiles at different dimensionless longitudinal distance $x/2r_j$ positions: 1) 4.0; 2) 10.0; 3) 20 for hydrogen-air mixing. Initial stream parameters and nomenclature are the same as those for Fig. 5.

somewhat nearer to the nozzle exit though in the whole flow region the combustion zone dimension can exceed the latter at ambient pressure. The hydrogen jet ignition process in air turns out to be rather sensitive to pressure levels in the mixing flows. For instance, the ignition of mixture under the same thermal conditions is not realized at $p = 0.5$ atm due to heat losses in the course of the mixing process during the induction stage. Furthermore, the "kinetic prehistory" of the mixing flows exerts a noticeable influence on ignition process behavior. Case 3 has been analyzed to clarify specifically a role of the intermediates in the ignition process. A critical regime was chosen to illustrate the competition between the heat losses that occur in the mixing process, and heat release due to chemical reactions. The initial parameters for mixing streams, the static temperature and the mixture composition were obtained from calculations of the equilibrium composition at a given fuel-air ratio and are presented in Table 3, Case 4. The ignition process of hydrogen jet in air activated by heating without molecular component concentration changes was analyzed numerically to draw a comparison. It is seen from Fig. 7 that the ignition occurs in the first case and is quenched in the second one. A good agreement between the theoretically and the experimentally observed positions of the visible flame boundary [9] confirms the validity of relaxation processes taken for modelling of the studied combustion system.

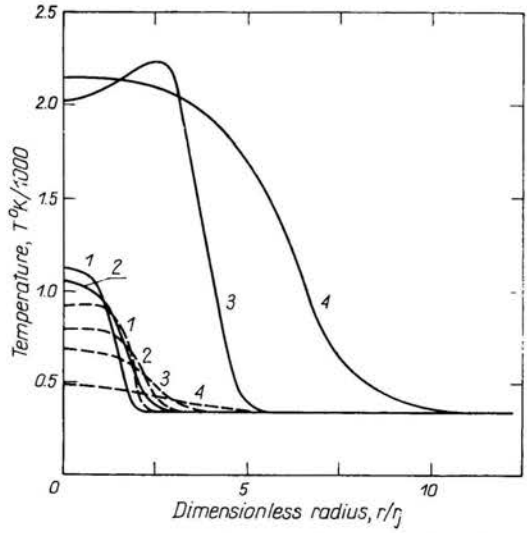

FIG. 7. Radial temperature profiles at different dimensionless longitudinal distance position for hydrogen-air mixing. Solid lines are for flow parameters of Case 3. The line numeration reffers to positions as follows: 1) 3.03; 2) 7.0; 3) 13.59; 4) 35.14. Dotted lines are for flow parameters of Case 4. The line numeration refers to positions $x/2r_j$ as follows: 1) 3.03; 2) 7.0; 3) 12.15; 4) 30.19.

3.2. Turbulent HF-chemical laser analysis

The primary problem in CW chemical laser system developments is to determine the optimal conditions for chemical energy transformation into energy of molecular excitation of active molecules on the base of accurate accounting of the reciprocal interaction between the flow transport, chemical reactions and the radiation fields, [13].

Below are presented the numerical results illustrating the efficiency of chemical energy transformation in a HF-laser in a case of continuous mixing of gaseous reactants in a turbulent nozzles/injectors system that provides high mixing rates at cavity pressure levels of 30–50 torrs. (The other aspects of the turbulence effect are not considered here). The experiments of [14] confirm that a well developed turbulent regime exists in the nonequilibrium gas flow under these pressures. Gas flows of similar configurations are employed in the mixing CO_2-N_2 GDL's in which the "pumping" gas, the hot nitrogen transfers its energy to the cold molecular system, a mixture of CO_2/He injected in the mixing region, [15].

Table 4. Reaction rate coefficients for HF-laser.

REACTION No.	REACTION	REACTION RATE COEFFICIENTS *) $K = aT^{\beta}\exp(-C/T)$			
		FORWARD (f) BACKWARD (b)	a	β	C, °K
1	$H_2 + F \rightleftharpoons HF(0) + H$	f	9.0×10^{12}	0	0.808
2	$H_2 + F \rightleftharpoons HF(1) + H$	f	1.8×10^{12}	0	0.808
3	$H_2 + F \rightleftharpoons HF(2) + H$	f	9.0×10^{13}	0	0.808
4	$H_2 + F \rightleftharpoons HF(3) + H$	f	4.5×10^{13}	0	0.808
5	$HF(2) + HF(0) \rightleftharpoons HF(1) + HF(1)$	b	3.0×10^{7}	1.5	0
6	$HF(2) + HF(1) \rightleftharpoons HF(0) + HF(3)$	f	2.8×10^{8}	1.5	0
7	$HF(2) + HF(2) \rightleftharpoons HF(1) + HF(3)$	f	8.38×10^{7}	1.5	0
8	$HF(3) + M_1 \rightleftharpoons HF(2) + M_1$	f	1.18×10^{1}	3.6	0
9	$HF(3) + M_2 \rightleftharpoons HF(2) + M_2$	f	1.5×10^{8}	1.3	0
10	$HF(2) + M_1 \rightleftharpoons HF(1) + M_1$	f	7.78×10^{-2}	3.6	0
11	$HF(2) + M_2 \rightleftharpoons HF(1) + M_2$	f	1.0×10^{8}	1.3	0
12	$HF(1) + M_1 \rightleftharpoons HF(0) + M_1$	f	3.89×10^{-2}	3.6	0
13	$HF(1) + M_2 \rightleftharpoons HF(0) + M_2$	f	5.0×10^{5}	1.3	0
14	$HF(0) + M_3 \rightleftharpoons H + F + M_3$	b	6.4×10^{-5}	-1.62	0.503
15	$HF(1) + M_3 \rightleftharpoons H + F + M_3$	b	6.4×10^{-5}	-1.62	0.503
16	$HF(2) + M_3 \rightleftharpoons H + F + M_3$	b	6.4×10^{-5}	-1.62	0.503
17	$HF(3) + M_3 \rightleftharpoons H + F + M_3$	b	6.4×10^{-5}	-1.62	0.503
18	$H + H + M_3 \rightleftharpoons H_2 + M_3$	f	7.5×10^{18}	-1.0	0
19	$F_2 + M_3 \rightleftharpoons F + F + M_3$	f	5.0×10^{13}	0	17.65
20	$H + F_2 \rightleftharpoons HF(0) + F$	f	6.0×10^{12}	0	1.2
21	$H + F_2 \rightleftharpoons HF(1) + F$	f	6.0×10^{12}	0	1.2
22	$H + F_2 \rightleftharpoons HF(2) + F$	f	9.0×10^{12}	0	1.2
23	$H + F_2 \rightleftharpoons HF(3) + F$	f	1.3×10^{13}	0	1.2

*) THE UNITS OF THE RATE COEFFICIENTS ARE: $cm^3 mole^{-1} sec^{-1}$ — FOR BIMOLECULAR REACTIONS, $cm^6 mole^{-2} sec^{-2}$ — FOR TRIMOLECULAR REACTIONS; T IS ABSOLUTE TEMPERATURE IN K DEVIDED BY 1000; M_1 — INERT DILUENT, M_2 - $\sum_v HF(v)$, M_3 - THE SUM OF ALL SPECIES..

Optical properties of the active medium containing the vibrationally excited HF(v) molecules are characterized by the stimulated emission intensity, and a small signal gain coefficients for the inverted *P*-branch transition of the electric dipole emission. The total and spectral line energies are also estimated provided the radiative and collisional processes are not coupled through the active medium parameters.

Figure 8 shows the schematic diagram of a hydrogen fluoride supersonic diffusion laser (SDL). Molecular hydrogen and fluorine are combusted in a plenum section to produce atomic fluorine. The expansion of reaction products through a supersonic nozzle array "freezes" the atomic fluorine which is then mixed and reacts in the downstream area thus producing the vibrationally excited molecules of HF(v). The chemical reactions in the mixing zone lead to the population inversion of various vibration-translationally excited states of active molecules, HF(v), which are then deactivated by collisions and radiation. The kinetic model is believed to describe the performance of HF-chemical laser as listed in Table 4. Exothermic ($\Delta H_R^0 = -31.6$ kcal/mole) reactions of cold "pump-

ing" between H_2 and F (reactions 0–3) lead to the population inversion of the first three vibrational levels of the excited HF-molecules ($v = 0, 1, 2, 3$). Highly exothermic ($\Delta H_R^0 = -98$ kcal/mole) "hot" reactions between H and F_2 (reactions 20–23) pump six vibrational levels ($v = 0, 1, \ldots, 6$), and the excited HF(v) molecules serve as the energy reservoir. Furthermore, the vibrational energy is (1) redistributed between the internal degrees of freedom of active molecules due to the resonance V–V energy transfer (reactions 5–6), (2) transformed into the translational energy of arbitrary molecules and atoms of the mixture by means of the V–T processes (reactions 7–13). It is also considered that in the dissociation model the reactions of HF(v)-molecules are either in ground or excited states. It is assumed that the mixture components have different characteristic efficiencies in the V–T deactivation processes. Relatively slow V–V deactivation reactions of molecular hydrogen are not considered in our scheme. The numerical values of the reaction rate coefficients used in this study were taken from [16].

Optical properties of vibrationally relaxing medium are expressed by means of a small signal gain coefficient for the inverted P-branch transition $v', j' \to v, j$ ($v' = v+1$, $j' = j-1$) of the vibration-translational spectrum of HF-molecule. For lasing to occur at the transition frequency ν_{vj} it is necessary for the gain, $g_{vj}^{v'j'}$, to exceed some threshhold value determined by cavity losses. The usual assumptions are made in the optical gain calculations. The presence of rotational equilibrium leads to the relation of the total population in the vibrational level v with the v, j sublevel population in the form

$$n_{vj} = n_v \frac{2j+1}{Q_R(v)} e^{-\alpha_v j(j+1)},$$

$$j = 0, 1, \ldots, \quad v = 0, \ldots, 3, \tag{3.1}$$

where

$$Q_R(v) = \sum_{j=0}^{\infty} (2j+1) e^{-\alpha_v j(j+1)}, \qquad \alpha_v = \theta_R(v)/T.$$

Here $\theta_R(v)$ is the characteristic rotational temperature for level v; T is the translational temperature of the mixture. For the pure Doppler broadened line the P-branch transition gain coefficients are written as follows:

$$g_{vj}^{v+1,j-1} = \frac{8\pi^{5/2} N_A j \varrho}{3h(2R_0 W_0 T \ln 2)^{1/2}} |M_{vj}^{v+1,j-1}|^2 \times \frac{1}{Q_R(v)} e^{-\alpha_v j(j+1)} [E_{vj}^{v+1,j-1} Y(v+1) - Y(v)], \tag{3.2}$$

where

$$E_{vj}^{v+1,j-1} = \frac{Q_R(v)}{Q_R(v+1)} e^{\alpha_v j \left[(j+1) - (j-1)\frac{\alpha_{v+1}}{\alpha_v}\right]}. \tag{3.3}$$

Here N_A is the Avagadro number, h is the Planck's constant, R_0 is the universal gas constant; W_0 is the molecular weight of active molecule; $|M_{vj}^{v+1,j-1}|^2$ are the matrix elements of the dipole moment for the stimulated emission or absorption. The values of $|M_{vj}^{v+1,j-1}|^2$ and other parameters of the active medium employed in [16] were used in the present

study. (The usage of other line shape functions does not essentially complicate the numerical procedure).

In a uniform medium the transition of the largest gain has the j-value determined by the Boltzman form of rotational distribution according to the relation

$$\alpha_v j_{\max}(2j_{\max}-1) = 1, \tag{3.4}$$

i.e., it is equal to 3 or 4. In a medium with essential spatial non-uniformity of parameters, the relation (3.4) is not valid. The so-called phenomenon of j-shifting is usually associated with the rapid mixture parameters' changes [17].

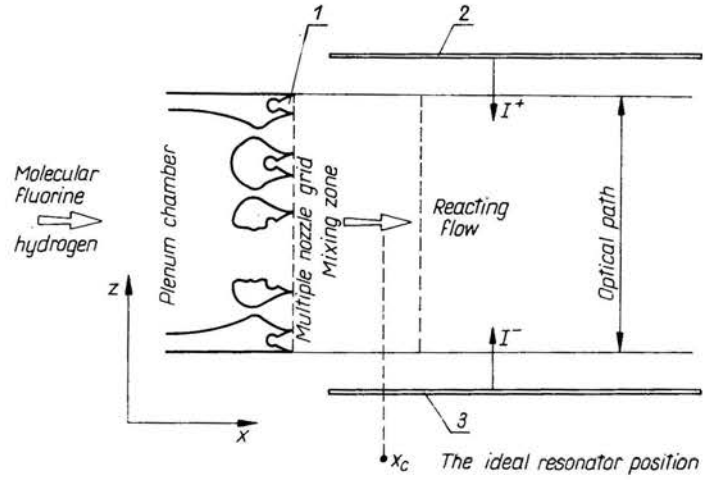

FIG. 8. Schematic diagram of a combustion-driven hydrogen-fluoride supersonic diffusion laser.

The maximum available optical energy is estimated by reducing to zero all the lasing transitions similarly to [16]. It is assumed that the Fabry-Perot cavity has an infinitesimal longitudinal length in the flow direction, i.e., it is located at a given axial position, x_c, as shown in Fig. 8. The deactivation by radiation is neglected in comparison with deactivation by collisions in the flow region before the cavity. In the longitudinal position x_c the gain coefficients are reduced to zero in all the lasing transitions due to $I_{vj}^{v'j'} \to \infty$ stimulated emission, and the total energy at x_c is obtained as being associated with the complete population inversion destruction. After assuming that the active molecules originally produced by chemical reactions have rotational distribution (3.1) at the local translational temperature and vibrational distribution with the total population inversion on bands 2/1 and 1/0 it is easy to determine the total number of molecules undergoing transitions between $(2,j) \to (1,j+1) \to (0,j+2)$ states of an active HF-molecule. (The calculations confirm the availability of such a situation). The number of single-quantum transitions is determined from

$$\Delta_{10} = \sum_{j=-1}^{\infty} \Delta_{10,j},$$
$$\Delta_{10,j} = n'_{0,j+2} - n_{0,j+2} = n_{1,j+1} - n'_{1,j+1} \tag{3.5}$$

where n_{vj} is the population of (v,j) state after lasing on $v/v-1$ band.

The zeroth gain coefficient at the distinguished P-branch transition means that

$$(2j+3)n'_{vj} = (2j+1)n'_{v-1,j+1}. \tag{3.6}$$

From the definition of $\Delta_{10,j}$ and from Eqs. (3.1) and (3.6) it is easy to obtain that

$$\Delta_{10,j} = N_A \frac{(2j+3)(2j+5)}{4j+8} \times \left[\frac{Y(1)}{Q_R(1)} e^{-\alpha_1(j+1)(j+2)} - \frac{Y(0)}{Q_R(0)} e^{-\alpha_0(j+2)(j+3)} \right], \quad j = -1, 0, 1, \ldots. \tag{3.7}$$

Defining numbers of single-quantum $\Delta_{21,j}$ and double-quantum transitions between the above mentioned states on 2/1, 2/0 and 1/0 bands, similarly

$$\Delta_{21,j} = n''_{1,j+1} - n'_{1,j+1},$$

$$\Delta_{20,j} = n''_{0,j+2} - n'_{0,j+2}$$

and accounting that

$$\Delta_{20,j} + \Delta_{21,j} = n_{2j} - n''_{2j}$$

after some algebra one can find

$$\Delta_{20,j} = \frac{2j+5}{2j+3} \Delta_{21,j}; \tag{3.8}$$

$$\Delta_{21,j} = \frac{(2j+1)}{3} N_A \left\{ \frac{Y(2)}{Q_R(2)} e^{-\alpha_2 j(j+1)} - \frac{1}{4j+8} \left[\frac{Y(1)(2j+3)}{Q_R(1)} e^{-\alpha_1(j+1)(j+2)} - \frac{Y(0)(2j+5)}{Q_R(0)} e^{-\alpha_0(j+2)(j+3)} \right] \right\}, \quad j = 0, 1, \ldots, 15.^{*)} \tag{3.9}$$

Here n''_{vj} is the population in v-level after lasing on 2/1 and 2/0 bands; $Y(v)$ is the mass concentration of excited molecules HF(v).

Thus, under the condition of a complete destruction of local population inversion between analyzed v-states the sum $\sum_{v=0}^{3} n_v$ of active molecules ($n_3 \ll n_v$, $v = 0, 1, 2$) generates $\Delta_{10,-1} + \sum_{j=0}^{15} (\Delta_{10,j} + 2\Delta_{20,j} + \Delta_{21,j})$ photones. Here the quantities $\Delta_{10,j}$, $\Delta_{20,j}$ and $\Delta_{21,j}$ are determined by the relations (3.7)–(3.9). Hence, the upper limit of an available radiative energy can be estimated as follows:

$$E(x_c) = N_A h \frac{\varrho}{W_0} \sum_{v=0}^{2} \sum_{j=0}^{15} \delta_v Y_v \nu_{vj}, \tag{3.10}$$

*) Fifteen j-sublevels are taken into account,

where

$$\delta_0 = \frac{1}{Q_R(0)}\left[\frac{4}{3}e^{-2\alpha_0} + \sum_{j=0}^{15}\frac{(2j+5)(6j+5)}{3(2j+3)}e^{-\alpha_0(j+2)(j+3)}\right],$$

$$\delta_1 = \frac{1}{Q_R(1)}\left[\frac{4}{3}\sum_{j=0}^{15}e^{-\alpha_1(j+1)(j+2)} + \frac{3}{4}\right], \tag{3.11}$$

$$\delta_2 = \frac{1}{Q_R(2)}\sum_{j=0}^{15}\frac{(2j+1)(6j+13)}{3(2j+3)}e^{-\alpha_2 j(j+1)}.$$

The ratio of the maximum available radiative energy to the total heat release occuring as a result of the pumping reactions determines a dimensionless coefficient of energy conversion:

$$\eta_u = E(x_c)\Big/\sum_{v=0}^{3}(\Delta h_v^0)Y(v)\frac{W_0}{W}. \tag{3.12}$$

It follows that the chemical efficiency of the laser system is equal to

$$\eta = \eta_u/(1+\eta_u).$$

The integral of gain coefficient taken along the optical path yields the ratio of output to input radiation intensities:

$$G_{vj}^{v'j'} = \frac{I_{\text{out}}(x)}{I_{\text{in}}(x)} = 2\int_{r_I}^{r_E} g_{vj}^{v'j'}(y)dy. \tag{3.13}$$

The above quantities are used to evaluate the energy conversion efficiency in the laser system under study. In spite of the complicated nature of the overall relaxation processes that govern the efficiency of the energy conversion in SDL it is possible to emphasize the following principal regularities. The pumping reaction rates and $V-V$ exchange processes are controlled mainly by initial laser stoichiometry and the mixing rate of initially unpremixed reactants. Rates of V—T energy transfer processes are not limited by mixing rates since the collisional partner for HF(v) is weakly dependent on its nature (with accuracy of cathalic efficiency). The mixture temperature and pressure become controlling factors (CF) for such reactions. At low temperatures a resonance V—V deactivation prevails. The non-isothermicity of the reacting system complicates considerably the competition between pumping and collisional processes. The evaluation of CF-optimal values and mixing rates are considered to be a matter of the practical interest.

The centerline selected optical gain $g_{vj}^{v'j'}$, ($v = 1$, $j = 4$) and the dimensionless coefficient of energy conversion distributions are presented in Fig. 9. Curves numerated according to the pressure increase, 2–4, manifest the variation of medium optical properties ($p_2 = 19$ torr, $p_3 = 38$ torr, $p_4 = 76$ torr) for Case 5. The effect of such a pressure variation appears in an increase of the maximum optical gain coefficients and shortening of an active region size. The maximum value of the energy conversion coefficient η_u is weakly dependent on the pressure level with emphasizes a slight effect of termolecular processes.

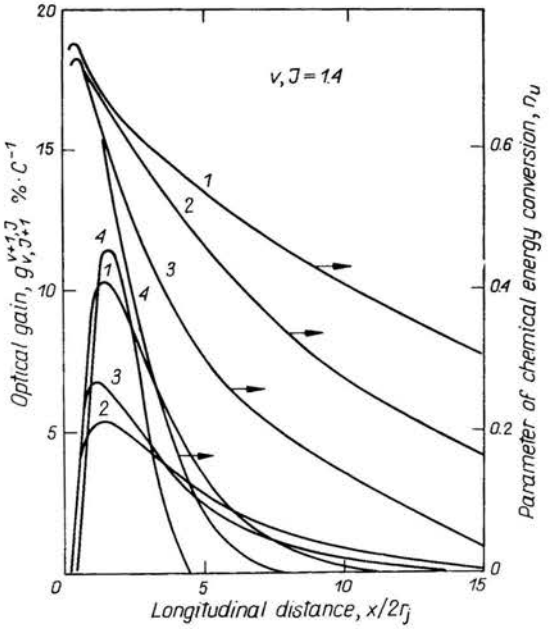

FIG. 9. Effect of pressure level (curves 2–4) and initial fluorine mass fraction (curve 1, $p = 19$ mm) on centerline mixture optical properties distributions for turbulent HF-chemical laser. (Case 5, Table 3)

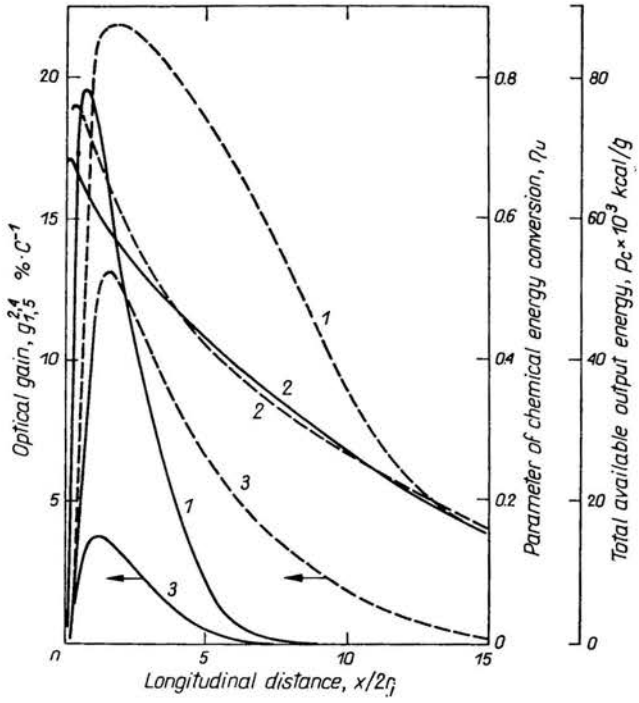

FIG. 10. Effect of initial jet temperatures on centerline mixture optical properties distributions under the pressure level of 38 mm for turbulent HF-chemical laser. Dotted lines reffer to Case 5, solid lines — to Case 6. Curve 1 is for the total available energy P_c.

In a regime of "cold" pumping a role of 19–23 stages is also restricted. Curve 4 (Case 6) presents the effect of mass flow rates F/H_2 in mixing streams. Although this case is an improvement of laser characteristics it is not generally valid. The initial stoichiometry affects the variation of the mixture temperature that changes relative rates of the whole complex of collisional processes. The affect of initial stream temperature variations (Case 7) on the same parameters of mixture is presented in Fig. 10. In comparison with Case 5 the essential deterioration of laser parameters is obvious. Moreover, the regime (Case 7) is characterized by the lower peak value of the total output energy and shortening of an active region size to be of great importance for a system with a real cavity. Hence the mixture temperature rise causes optical characteristics to become inferior due to removal from a maximum total inversion state. CF-values can be "optimized" by means of gasdynamic control. The variation of the initial stream jet velocities' ratio is proved to be rather effective as illustrated in Fig. 11. Here the comparison of laser characteristics for Cases 5 and 8 are presented.

Figure 12 (Case 5, $p = 76$ torr) shows a collisional cascading effect to be available due to a difference in specific times of population inversion destruction on 2/1 and 1/0 bands. Radial distributions of optical gain coefficients for selected transitions on 2/1 and 1/0 bands can be described by inequality $g_{0,j}^{1,ji} < g_{1,j}^{2,ji}$. In the downstream flow region these coefficients manifest a qualitatively opposite behavior, as also seen in Fig. 12. The transversal size of a positive gain region for transition on 1/0 band turns out to be considerably lar-

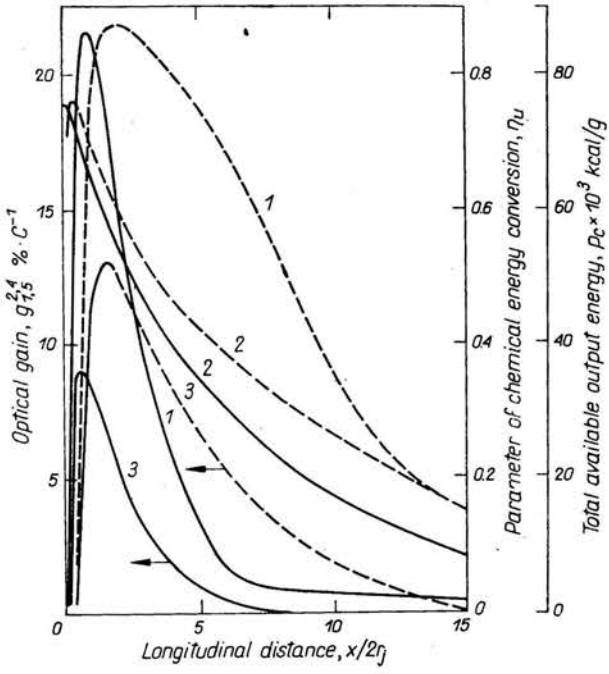

FIG. 11. Effect of initial jet velocities ratio on centerline mixture optical properties distributions under the pressure level of 38 mm. The comparison of 5 and 7 cases are presented. Curve 1 is for the total available power P_c.

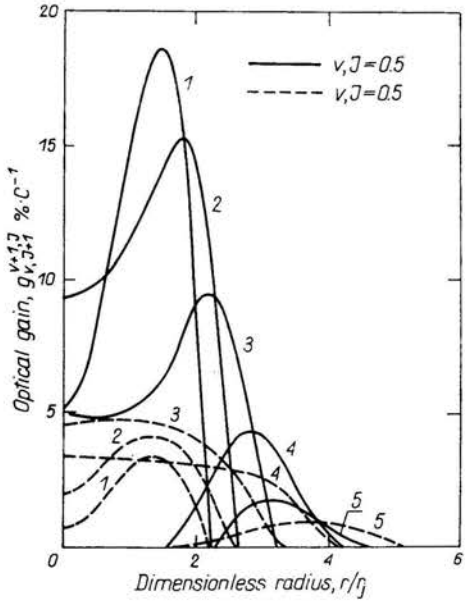

FIG. 12. Effect of collisional cascading on the radial optical gain distributions under the pressure level of 76 mm (Case 5) at the different dimension longitudinal positions, x: 1) $0.292 \cdot 10^{-3}$m; 2) $1.048 \cdot 10^{-3}$m; 3) $3.131 \cdot 10^{-3}$m; $5.508 \cdot 10^{-3}$ m; 5) $9.27 \cdot 10^{-3}$m.

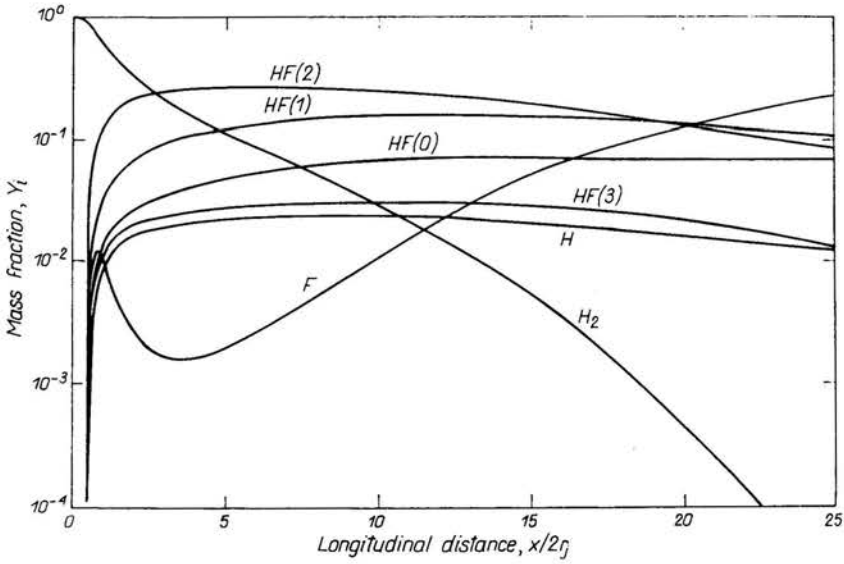

FIG. 13. Centerline chemical composition histories for turbulent HF-chemical laser (Case 5, p = 76 mm).

ger. The optical gain coefficient distribution for such a transition is characterized by a lower degree of non-uniformity. Non-uniformity of optical properties is generally caused by non-uniformity of thermochemical mixture parameters. Chemical composition and radial temperature profiles are plotted in Figs. 13 and 14. The temperature of mixture is increased up to a level considerably exceeding the initial one due to the exothermicity of pumping reactions and the posterior effect of V—T relaxation processes. As it follows from concentration distributions a total inversion exists initially on both 2/1 and 1/0 bands,

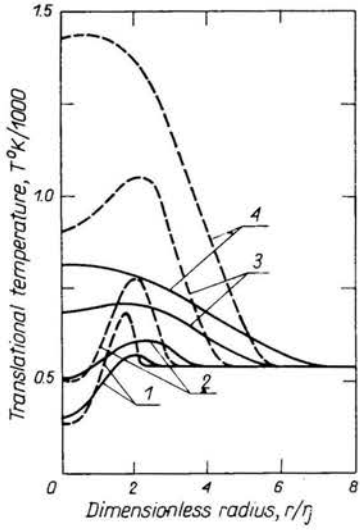

FIG. 14. Radial translational temperature profiles at different dimensionless longitudinal distance $x/2r_j$ positions: 1) 1.048; 2) 2.50; 3) 7.0; 4) 12.93. Dotted lines correspond to the flow containing nitrogen as an inert diluent, solid lines — helium. (Case 5, 8).

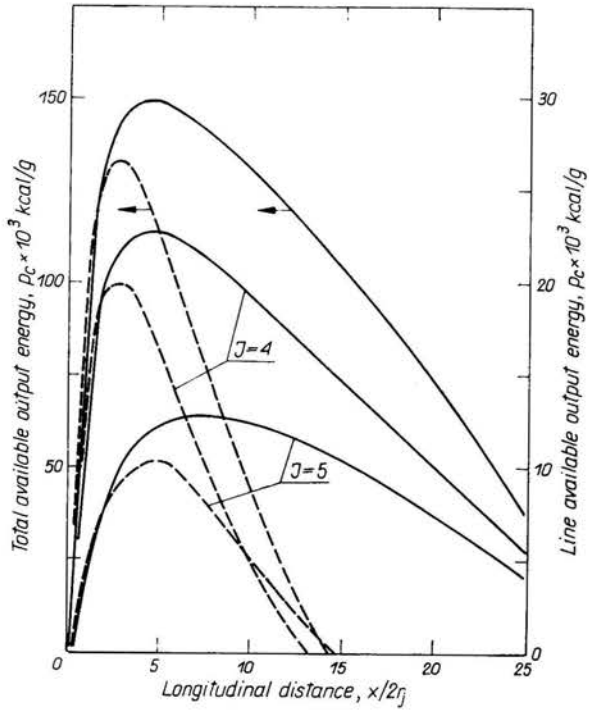

FIG. 15. Effect of an inert diluent kind on mixture energetic properties for turbulent HF-chemical laser. The flow parameters and nomenclature are the same as for Fig. 14.

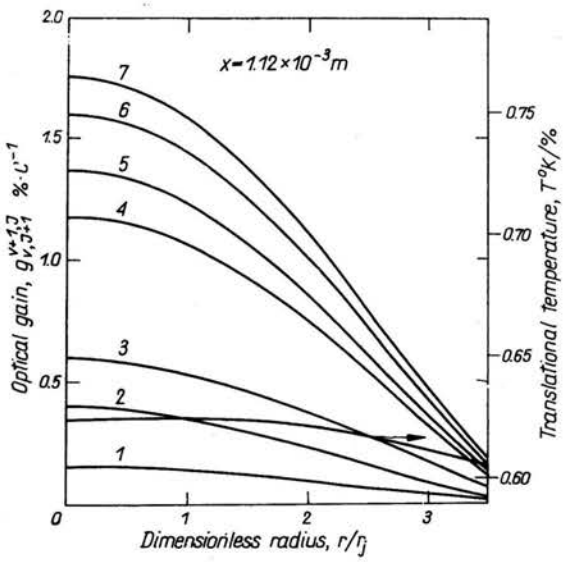

FIG. 16. The absence of the *j*-shift phenomenon for streams containing a large inert diluent mass fraction. The initial parameters are the same as for Case 5, but Y_{N_2} equals 0.9 in both streams, $p = 19$ mm.

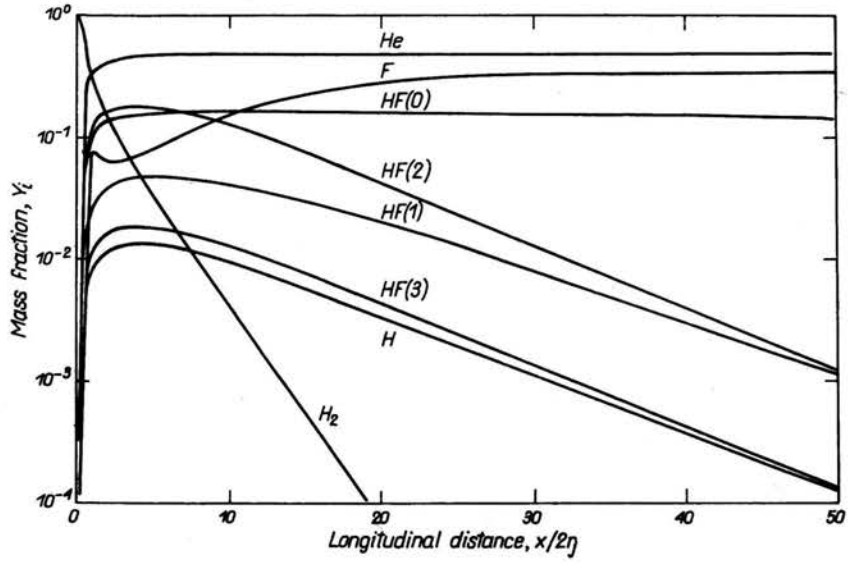

FIG. 17. Centerline chemical composition histories for combustion-driven turbulent HF-chemical laser (Case 9, $p = 19$ mm).

i.e. $n_1, n_2 > n_0$. A partial inversion on 3/2 band, $n_3 < n_v$, $g_{2,j+1}^{3,j} \geqslant 0$, exists only at the beginning of a mixing zone. It proves sufficiently an assumption introduced for the output energy evaluation. The effect of thermal condition change in a case of helium displacing nitrogen as a diluent is clearly illustrated in Fig. 15. Calculations confirm the well-known experimental facts of advantaged low-temperature operation under such a condition.

A spatial non-uniformity of thermochemical mixture properties leads to the j-shift phenomenon, i.e., the j-number for the transition with the maximum optical gain coefficient consequently differs by 1 during the process development. In this case it is possible

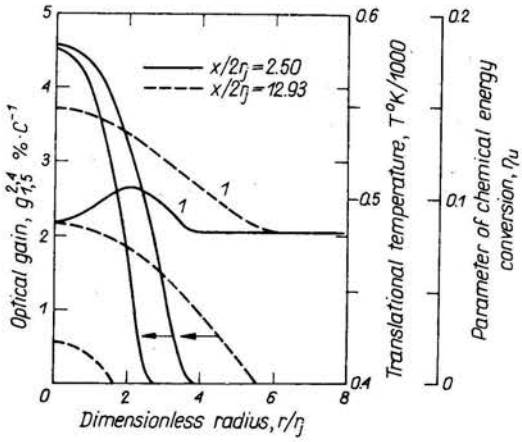

FIG. 18. Radial mixture translational temperature and optical properties distributions for combustion-driven HF-chemical laser (Case 9, p = 19 mm). Curve 1 is for mixture translational temperature.

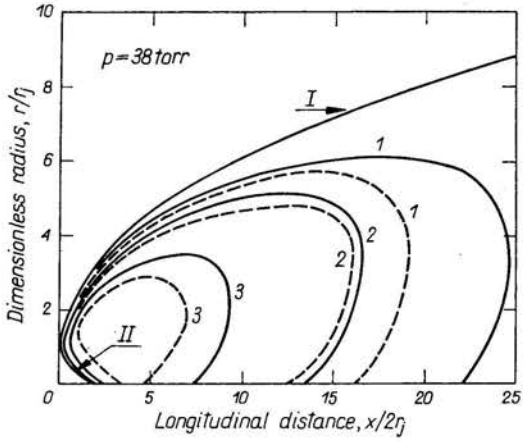

FIG. 19. Boundaries of a mixing zone and isogain lines in the flowfield of turbulent combustion-driven HF-chemical laser. *I*, *II* are the outer and inner boundaries, respectively. Solid lines correspond to g_{15}^{24} transition, dottet lines — g_{17}^{26}; 1) 1% cm^{-1}, 2) 2% cm^{-1}, 3) 5% cm^{-1} ratios (p = 38 torr, T_j = 540°K, mass fraction in the outer stream are *F*: *HF(O)*: *He* = 4:1:5. Other parameters are the same as for Case 9).

to observe a forward j-shift, i.e., $j \to j+1$, as well as a backward one, i.e., $j \to j-1$. The longitudinal size of an active region appears to be stretched for a large j-number transition due to the presence of a forward j-shift. The latter does not occur in the near isothermal flow as presented in Fig. 16 (Case 5, reactant streams are highly diluted with nitrogen).

Flow processes play an important part in laser action development. The choice of the turbulent mixing model is proved to be an essential factor of valid prediction. It is instructive to note that a model in a form (3) requires the "optimization" of specific constants for the flow with an axial symmetry.

In the computational model described above, the question of oxidizing medium to be created is practically open since attention is focused on "cold" HF-system with fully dissociated fluorine. The degree of dissociation is not considered as a parameter. Typical characteristics of the energy conversion process produced by combustion — heated version of SDL are presented in Figs. 17–19. It is concluded that the active medium produced by means of a combustor-scheme has worse energy conversion characteristics.

4. Conclusions

It is clearly illustrated that complicated, nonequilibrium chemically-reacting flow problems can be successfully analyzed to a sufficient extent of validity. The obvious trends exist in approaching theoretical models of combustion and practical systems. The analysis of a more complicated nonequilibrium system similar to reacting flows of CW chemical lasers is directly effected by the combustion process study. The usage of extremely fine turbulent injectors in SDL-flows is resulted in the cavity pressure increase up to the level of decades of torrs together with the gasdynamic control in maintaining the proper operating conditions. The efficiency of chemical energy conversion (i.e., 32 kcal/mole) is found not to exceed 8–10 per cents. The initial gas stream temperatures as well as the exothermicity caused by thermal effects of pumping reactions are the limiting factors. The usage of low-molecular-weight diluents and the low-temperature operating condition is proved to be useful. The numerical analysis predicts the cascading effect as well as the high spatial non-uniformity of optical parameters that elucidate difficulties in achieving of a sufficient beam quality.

The applications of an "exact" model of turbulence together with the rate coefficients for a chemical model of laser action are required to present valid predictions.

The displacement effect due to the mixing layer development can be considered additionally in the present computer program.

Acknowledgments

The extensive contributions and continued support of Professor R. I. SOLOUKHIN and the useful investment of Professor S. WOJCICKI are greatly acknowledged.

References

1. F. A. WILIAMS, *Combustion theory*, Nauka, Moskva 1971.
2. C. E. PETERS, D. E. CHRISS, R. A. PAULK, *Turbulent transport properties in subsonic coaxial free mixing systems*, AIAA Paper, 69–681, 1969.
3. B. E. LAUNDER, D. B. SPALDING, *The numerical computation of turbulent flows*, Computer Methods in Applied Mechanics and Engineering, 3, 269–289, 1974.
4. B. E. LAUNDER, D. B. SPALDING, *Mathematical models of turbulence*, Academic Press, London 1972.
5. S. V. PATANKAR, D. B. SPALDING, *Heat and mass transfer in boundary layers*, 2nd ed., Intertext Books, 1970.
6. H. E. BAILEY, *Numerical integration of the equation governing the one-dimensional flow of a chemically reactive gas*, The Physics of Fluids, **12**, 11, 2292–2300, 1969.
7. C. SCACCIA, L. A. KENNEDY, *Calculating two-dimensional chemically reacting flows*, AIAA J., **12**, 9, 1268–1272, 1974.
8. R. BELLMAN, R. KALABA, *Quasi-linearization and nonlinear boundary-value problems*, Mir, Moskva 1968.
9. V. K. BAEV, V. I. GOLOVICHEV, V. I. DIMITROV, V. A. YASAKOV, *Calculation of ignition and combustion of a hydrogen jet in air with finite chemical reaction rates*, Astronautica Acta, **1**, 1227–1238, 1974.
10. R. W. DUFF, *Calculation of reaction profiles behind steady state shock waves*, I. *Application to detonation waves*, J. Chem. Phys., 28, 1193–1197, 1958.
11. O. BREVIG, F. SHAHROKHI, *On the free turbulent mixing and combustion between coaxial hydrogen and air streams*, AIAA Paper, 71–5, 1971.
12. D. L. BAULCH et al., *Evaluated kinetic data for high temperature reactions*, **1**, London 1974.
13. N. G. PREOBRAZHENSKY, *On the diffusion problems, arising in the linear theory of gasdynamic and chemical lasers*, PMTF, 2, 32–37, 1974.
14. W. L. SHACKLEFORD, A. B. WITTE, J. E. BROADWELL, J. E. TROST, T. A. JACOBS, *Experimental measurements in supersonic reacting* ($F+H_2$) *mixing lasers*, AIAA J., **12**, 8, 1009–1010, 1974.
15. V. N. CROSHKO, R. I. SOLUKHIN, P. WOLANSKI, *Population inversion by mixing in a shock tube flow*, Optics Communications, **6**, 3, 275–277, 1972.
16. W. S. KING, H. MIRELS, *Numerical study of diffusion-type chemical lasers*, **10**, 12, 1647–1654, 1972.
17. G. EMANUEL, *Analytical model for a continuous chemical laser*, JQSRT, 11, 1481–1520, 1971.

INSTITUTE FOR PURE AND APPLIED MECHANICS
ACADEMY OF SCIENCES, NOVOSIBIRSK, USSR.

Received September 16, 1975.